

Analysis of low-energy-electron-diffraction intensity spectra for (001), (110), and (111) nickel

J. E. Demuth, P. M. Marcus, and D. W. Jepsen

IBM Thomas J. Watson Research Center, Yorktown Heights, New York 10598

(Received 10 July 1974)

Elastic low-energy-electron-diffraction intensity-energy spectra are calculated for Ni (001), (110), and (111) surfaces between 10 and 220 eV by the layer-Korringa-Kohn-Rostoker method and compared with recent room-temperature experimental results. The calculation uses the Wakoh self-consistent muffin-tin potential, retains eight phase shifts, and includes finite temperature effects (assuming a Debye spectrum). An effective Debye temperature of 335 °K is found from the temperature dependence of spectral intensities, an energy-dependent imaginary potential roughly of the form $\beta = 0.85E^{1/3}$ for electron energy E (in eV) is determined by matching features of the calculated spectra to experiment, and the best values of the first interlayer spacing are found to be 1.76 Å (the bulk spacing) + 0.02 ± 0.02 Å on the (001) surface, 1.24 - (0.06 ± 0.02) Å on the (110) surface, and 2.03 - (0.025 ± 0.025) Å on the (111) surface. With these parameters, excellent agreement with observed spectra is obtained in positions and shapes of peaks for several beams and a large number of incident angles. For all faces a small systematic deviation in peak positions is found with a constant 11-eV inner potential, suggesting an inner potential varying from the expected static value of 13.5 at low energies to about 9 eV near 220 eV. Comparison of relative intensities between calculation with the above $\beta(E)$ and experiment suggests that excitation of 3p electrons from Ni significantly enhances electron absorption above 65 eV.

I. INTRODUCTION

Much recent progress has been made in achieving a quantitative theory of low-energy electron diffraction (LEED) and in obtaining structural information from LEED spectra.¹⁻⁶ A detailed analysis of the LEED spectra of clean Ni is particularly important because it provides the basis for studies of the LEED spectra of chemically adsorbed ordered overlayers of atoms or molecules on Ni single-crystal surfaces. Such studies are directed towards the determination of the adsorption site and bonding geometry of chemisorbed atoms and molecules—useful information in understanding the nature of surface chemical bonding.

With these goals in mind, we have examined in detail the recent room-temperature experimental LEED spectra of Demuth and Rhodin⁷ for the (001), (110), and (111) surfaces of nickel. The method used for these calculations, the layer-KKR method, applies the KKR (Korringa-Kohn-Rostoker) method of band theory to a single atomic layer to give the scattering properties of that layer, which are then used to solve the multiple-scattering problem between layers with a matrix procedure.² In the application to Ni we systematically determine the value of a single effective Debye temperature used in all layers, the values of the electron attenuation as a function of energy, the values of the inner potential as a function of energy, and the deviations of the first nickel interlayer spacing on each face from their bulk values. These energy-dependent values of the inner potential and absorption pro-

vide basic information about the effective one-electron potential for an excited electron in a real metal. These calculations are also compared with recent model calculations on clean Ni surfaces by Laramore⁸ and Tong and Kesmodel.^{5,6} Perturbation-type calculations on Ni, reported previously by Andersson and Pendry,⁹ Tait, Tong, and Rhodin,¹⁰ and Rhodin and Lee,¹¹ will not be discussed here. The first of these calculations covered a much narrower energy range, and the latter are felt to be less accurate because of the approximations employed.¹²

II. FEATURES OF MODEL

The layer-KKR method² for calculating LEED intensity versus energy curves or LEED spectra is applied here to a model which accurately treats multiple scattering within and between layers for a semi-infinite crystal, but neglects scattering produced by the potential barrier between vacuum and the first atomic layer; it is assumed that this barrier varies so smoothly that it causes negligible additional scattering (the no-reflection boundary condition). Inclusion of surface barriers has been shown to modify diffraction intensities primarily at very low energies ($E \lesssim 40$ eV),^{2,9,13,14} as well as to introduce sharp spectral features which can be associated with barrier resonances.¹⁵ Due to the irregularity of the surface on the atomic level, such resonance features are not expected to be observed in experimental spectra¹⁵ and the comparison of theory and experiment made here,

as well as in other work^{2,14} shows that suitable agreement can be achieved without including the details of the surface barrier. Although electron scattering from this barrier is neglected, changes in the electron momentum associated with crossing this barrier are included.

The LEED calculations to be presented here use eight phase shifts to describe the scattering potential of the Ni atom and up to 47 beams (29 beams minimum) in the representation of wave functions, so that the calculated intensity remains accurate to within 5% up to 220 eV. (We have also considered ten phase shifts in the calculation, but find that eight phase shifts are suitable below ~220 eV.) Since the calculation is based upon elemental layers, we can easily calculate additional spectra for 5 and 2.5% expansions and contractions of the first layer spacing (from the expected bulk interlayer spacing) with little additional computational time. The lattice spacing used for the semi-infinite crystal is based upon a bulk Ni lattice spacing of $a_0 = 3.517 \text{ \AA}$.

LEED intensities were calculated at 1-eV intervals from 10 to 220 eV so that the line shapes and peak positions of the LEED spectra could be compared with experiment in detail. Previous calculations^{5,8} for Ni have been based upon energy intervals of 2.5–5 eV, and have therefore not allowed detailed resolution of calculated line shapes. Such resolution of line shapes and peak positions becomes very important in assessing the choice of electron damping used in the model, the degree of surface expansion or contraction which occurs, as well as the possible variations in inner potentials with energy—all determined from comparison with experimental spectra. For 47 (29) diffraction beams (all found simultaneously), the calculation (which includes lattice motion and five different first interlayer spacings) takes 12 (3) sec per energy point per interlayer spacing and requires 850 (550) kilobytes of machine storage on an IBM 360/91.

By comparison of our eight-phase-shift calculation with calculations using five phase shifts we find, in agreement with Tong,⁶ that more than five phase shifts are needed to adequately describe several features of the room-temperature experimental spectra. From the relative magnitude of the $l \geq 4$ phase shifts for nickel above 80 eV (or even below 80 eV) it might be expected that inclusion of these phase shifts would not significantly affect the LEED spectra. Lattice motion, however, makes it necessary to include additional phase shifts in the calculation to describe the atomic scattering as modified by vibration. In our calculation the vibrating atoms are modeled as a rigid lattice of "blurred-atom" scatterers at each site.² We find that these blurred-atom scatterers

require more phase shifts than the fixed atom to accurately describe their scattering.

In Fig. 1 we compare five- and eight-phase-shift calculations, made with identical model parameters, for the (00), (01), and (11) beams on Ni(001) and demonstrate that above ~80 eV not only do peak shapes and fine structures differ, but peak positions are shifted by up to 8 eV between the two calculations. Above 80 eV the peak positions for the five-phase-shift calculation are systematically shifted to higher energies than those for the eight-phase-shift calculation. For certain peaks, such as the 160-eV peak in the (01) beam, using too few phase shifts alters the shape of the peak in such a manner as to *lower* the peak position. Thus we

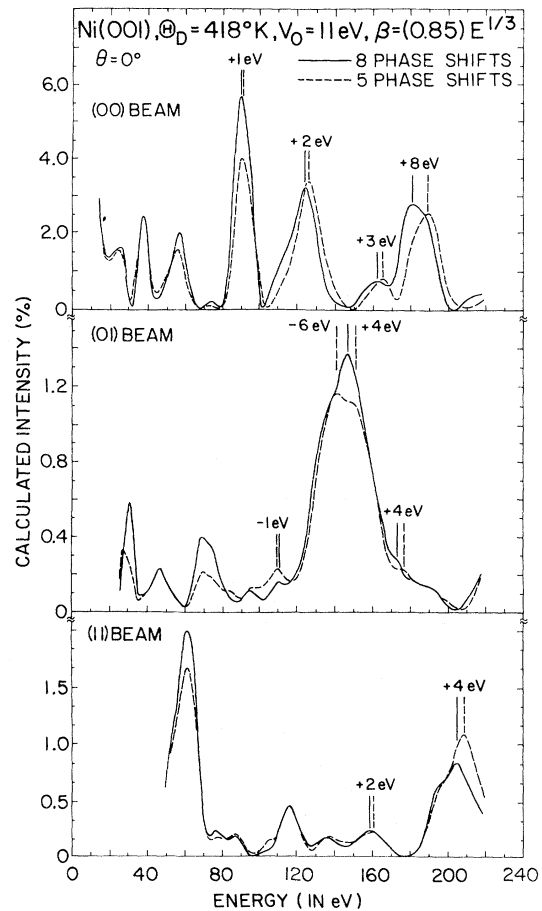


FIG. 1. Comparison of room-temperature LEED spectra calculated with five phase shifts (dashed line) and eight phase shifts (solid line) for the (00), (01), and (11) beams for a room-temperature semi-infinite Ni(001) surface at normal incidence ($\theta = 0^\circ$). The Wakoh potential for Ni and identical model parameters have been used in each calculation. The displacements in peak positions for the five-phase-shift calculation (dashed line) from the eight-phase-shift calculation (solid line) are indicated.

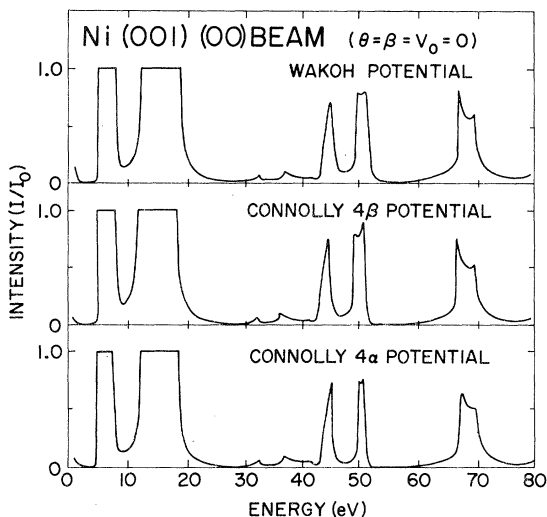


FIG. 2. Comparison of calculated LEED spectrum for the Wakoh potential (Ref. 20) and the ferromagnetic potential of Connolly (Ref. 19) for which we show both minority (β) and majority (α) spin components. The calculations are for the (00) beam at normal incidence, with zero absorption and inner potential.

conclude that above ~ 80 eV the peak positions and line shapes of a five-phase-shift calculation for Ni are inaccurate and can severely limit the agreement achieved between theory and experiment. We note that the spectra we have calculated with five phase shifts for a semi-infinite crystal are nearly identical to those calculated with five phase shifts for a five-layer crystal.^{5,8} (These latter calculations are based on Beeby's scattering formalism.¹⁶)

A. Scattering potential

Previous work on clean surfaces has shown that band-structure potentials do a satisfactory job of describing experimental data for clean surfaces.^{2,17} It has been shown for several clean surfaces^{2,17,18} that superposition potentials, i. e., superpositions of atomic potentials, also describe LEED data adequately. Since nickel is a ferromagnetic material and separate potentials are available for the two separate spin directions,¹⁹ we can also estimate the magnitude of ferromagnetic effects on the LEED spectra. Figure 2 displays calculated LEED spectra on Ni(001) (without electron absorption) for the self-consistent Connolly potential¹⁹ for both minority (β) and majority (α) spin distributions in Ni and for the Wakoh potential.²⁰ Without electron absorption the calculated LEED spectra show very small differences and, due to electron absorption in the real crystal, the spectra with absorption are even closer. Thus, in summary, we cannot distinguish such small differences in crystal potential by comparison with the experi-

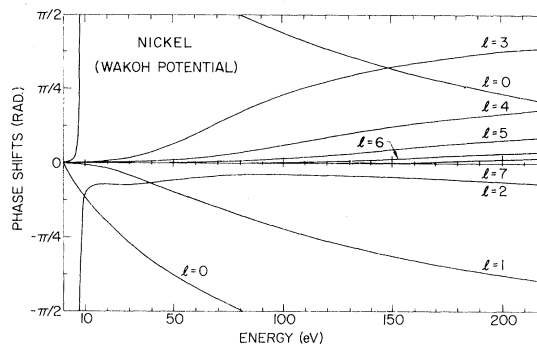


FIG. 3. Energy-dependent phase shifts δ_l for $0 \leq l \leq 7$ used to describe the Wakoh scattering potential (Ref. 20) for the calculations. The energy is measured from the muffin-tin zero.

mental LEED data, and we use the Wakoh potential in these calculations. The phase shifts obtained for this self-consistent band-structure potential are shown in Fig. 3.

B. "Inner potential"

To define the scattering potential completely for electrons incident from vacuum requires establishing the level of the muffin-tin zero for the Wakoh potential with respect to the vacuum level; this difference we call the "inner potential," V_0 , as shown in Fig. 4. We estimate an average value of

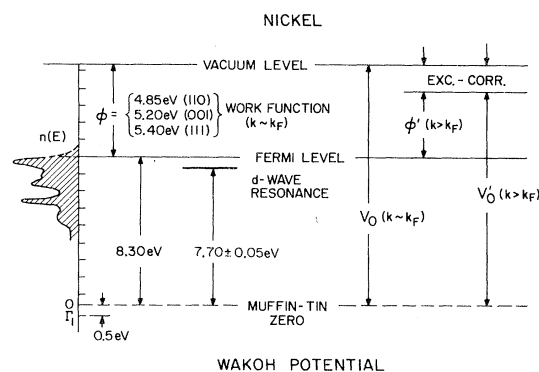


FIG. 4. Energy-level diagram for the Wakoh potential (Ref. 20), experimentally determined work functions for Ni (Ref. 7), and the bulk density of states for nickel (Ref. 20) (shown at left). The locations of the d -wave resonance (as determined from the energy at which the $l=2$ phase shift crosses through $\frac{1}{2}\pi$) and the Fermi level for this potential (as determined from band calculations) are shown with respect to the muffin-tin zero and the calculated bulk density of states. The static inner potential ($k \sim k_F$) is shown as the distance between the vacuum level and the muffin-tin zero. For higher incident-electron energies ($k > k_F$) the inner potential V_0 is expected to decrease (Refs. 2, 21).

$V_0 = 11$ eV over the energy range 20–150 eV from matching the peak positions of the nonspecular beams at normal incidence and of the specular beam at $\theta = 4^\circ$ (for both $\phi = 0^\circ$ and 45°) for the (001) surface.

A static estimate of V_0 of 13.2–13.7 eV can be obtained for the Wakoh potential by adding the Fermi-level position with respect to the muffin-tin zero, 8.30 eV, to the measured (static) work functions for the various surfaces of about 5 eV (see Fig. 4). However, we can expect that the effective inner potential decreases in magnitude for higher-energy electrons, since the magnitude of the correlation energy for electrons with energies well above the Fermi level will be reduced, as shown by detailed calculations of the self-energy of the uniform electron gas (jellium).²¹ Thus, comparison of calculated and experimental peak positions based on $V_0 = 11$ eV should show a systematic energy dependence. Indeed, we find a gradual decrease of V_0 from the static value at low energies (below ~ 30 eV) to ~ 9 eV at energies of ~ 220 eV, as will be discussed later.

C. Electron damping and effective Debye temperature

The effects of electron damping due to inelastic scattering processes in the solid and the effects of lattice motion must be included in the scattering model as well. Electron damping in the crystal is taken into account by supplementing the crystal potential with an imaginary part β , assumed spatially constant, but which can be made a function of energy. Lattice motion is introduced by averaging the scattering of the atom over the lattice motion at each site given by a Debye spectrum (this we refer to as the “blurred” atom), and then introducing the resulting average t matrix into the rigid-lattice formalism.^{2,22,23} Since these two parameters produce similar modifications in LEED spectral intensities, we have determined each input parameter using different experimental features of the LEED spectra.

1. Determination of Θ_D

The experimental temperature dependence of LEED intensities allows a direct determination of an effective layer-averaged surface Debye temperature. Here we compare the experimental temperature dependence to the calculated temperature dependence for different Debye temperatures for a given absorption to determine Θ_D . (The initial choice of electron damping does not strongly affect the calculated temperature dependence).²⁴ Within the framework of the model, which considers all layers to have equivalent vibrational properties, we find that a single Debye temperature of about 335 °K can be used to describe the experi-

mentally measured temperature dependence of intensities from (001), (110), and (111) surfaces.^{25–27} As shown in Fig. 5, although there is considerable spread in the few data points available, the effective value $\Theta_D = 335$ °K is more consistent with the temperature dependence of the diffraction intensities than bulk Θ_D 's of $\sim (420–440)$ °K.^{28,29} This reduced effective value of Θ_D is readily understandable in terms of the larger vibrational amplitudes of surface atoms compared to bulk atoms. {For example, values of mean square normal vibrations for the first five layers of a (001) surface³⁰ of Ni calculated using a nearest-neighbor central-force model and the harmonic approximation correspond to reducing the bulk Debye temperatures by $\sim 0.71, 0.88, 0.93, 0.96,$ and 0.98% [and similarly for a (110) or (111) surface].}

We have also examined the effects of increased surface vibrations for the first atomic layer on the room-temperature LEED spectra of Ni (001) by choosing $\Theta_D = 300$ °K for that layer and using the bulk value of $\Theta_D = 420$ °K for all other layers; we find that the LEED spectra are nearly the same as with use of a single effective layer-averaged Debye temperature of 335 °K. From comparing these latter two surface-vibration models, we find that at low energies (~ 40 eV) the intensities are nearly identical, while at higher energies ($\sim 150–200$ eV) the calculation using the effective Debye temperature of 335 °K yields intensities lower than the 300 °K surface Debye model by about (20–30)%. We might thus expect that our

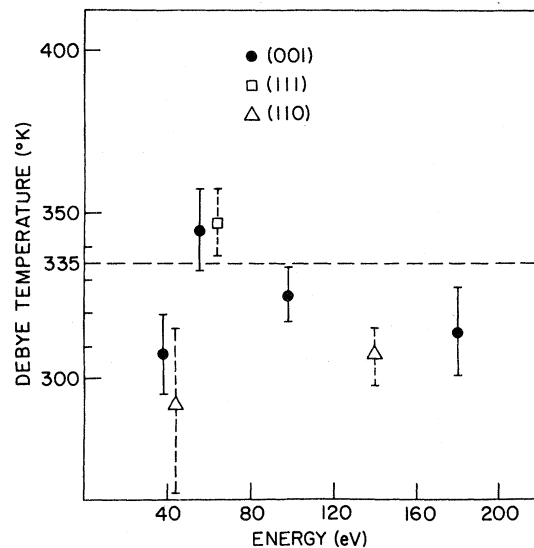


FIG. 5. Effective Debye temperatures used for all layers determined from matching the experimentally observed temperature dependence of the diffraction intensities for (001), (110), and (111) nickel (Refs. 25–27) to the temperature dependence obtained in the calculation.

use of a single effective Debye temperature would underestimate experimental diffraction intensities at these higher energies. One could also use layer-dependent Debye temperatures, as was done by Tong and Kesmodel,⁵ but such further refinements would appear to affect room-temperature spectral features negligibly and thus be unnecessary in the present analysis.

2. Determination of $\beta(E)$

After the effective Θ_D is found as described above, the values of the imaginary part of the potential β are determined phenomenologically by matching calculated and measured spectral line shapes, fine structure, and relative intensities in the spectra. By matching the shapes of both peak-shoulder combinations and intensity minima, values of β around particular energies are found; by matching relative peak intensities at low and high energies, the relative β values at low and high energies are found. In this way reasonable consistency not only of the structural features but also of the relative intensities is found with the function $\beta(E) = 0.85E^{1/3}$ (with β and E in eV)—as opposed either to constant- $\beta(E)$ or constant-electron-mean-free-path assumptions commonly used.^{1-5,8-13,18} This procedure for evaluating $\beta(E)$ avoids matching the absolute intensities (I/I_0) of calculated and measured spectra, which are affected by other features of the experiment, such as the surface roughness and the variation of the incident-beam coherence zone with energy. The constant of 0.85 in this expression was chosen from several values to provide the best fit to the experiments.

We note that the $E^{1/3}$ variation of β produces a λ_{ee} variation above 50 eV which is more consistent with the trends in λ_{ee} observed in low-energy-electron-mean-free-path variations with energy³¹ than with a constant mean free path. The $E^{1/3}$ dependence of β for Ni also agrees with values determined from kinematic theory for Ni for electron energies below ~ 40 eV.⁷ A similar $E^{1/3}$ dependence above 50 eV also was found in recent work on Ag by Jepsen, Marcus, and Jona¹⁴ where the difficulty caused by surface roughness in determining β was overcome by comparing the measured total elastic backscattering to the calculated total rigid-lattice backscattering at finite absorption. This procedure assumes that both roughness and lattice motion merely redistribute the scattered electrons, which are all in sharp beams for a rigid lattice, as diffuse background over the collection hemisphere.

We have similarly analyzed the total integrated elastic-backscattering measurements from Ni(111) that were obtained by Lagally and Webb.³² A com-

parison of our calculated total rigid-lattice backscattering to their data on Ni(111) leads to a set of β values as a function of energy (~ 6 eV at 100 eV and 9.5 eV at 200 eV) which when used in our calculation leads to strong washing out of spectral details, suggesting that such an absorption function is too large. A previous analysis of Lagally and Webb's LEED data on Ni(111)⁸ and comparisons to other experimental data⁷ suggest that their measured intensities may be too low.³³ Such intensity differences would lead us to overestimate β .

In Fig. 6 we compare the function $\beta(E) = 0.85E^{1/3}$

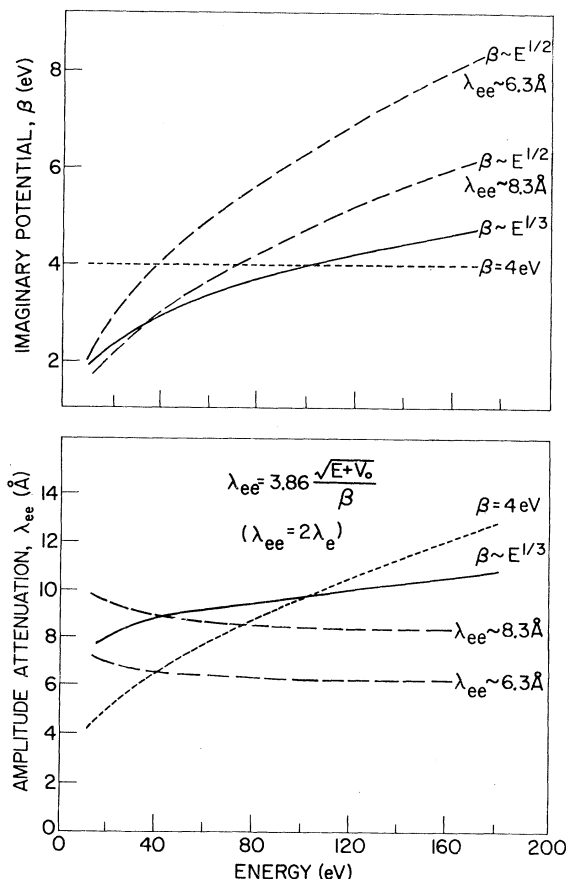


FIG. 6. Energy dependence of the imaginary component to the potential, β (top), and corresponding amplitude attenuation coefficient, λ_{ee} (bottom), for several possible choices of the parameter used to describe the electron damping in the scattering model. Both constant-damping (β) and nearly-constant-amplitude-attenuation-coefficient (λ_{ee}) assumptions are shown as well, as a $\beta(E) = 0.85E^{1/3}$ absorption function which allows the best overall description of the fine structure in the experimental spectra. The energy scale is referenced in both cases to the vacuum level. (The intensity attenuation coefficient, λ_e , is more commonly the quantity obtained in electron mean-free-path determinations and is equal to one-half the amplitude attenuation coefficient, λ_{ee} .)

with the $\beta(E)$ corresponding to a nearly-constant electron amplitude attenuation with λ_{ee} values of ~ 6.3 and ~ 8.3 Å (Laramore⁸ used $\lambda_{ee} = 8$ Å) and with a constant β of 4 eV. For a plane wave of energy E propagating in a uniform absorbing medium, β is related to the amplitude attenuation coefficient, λ_{ee} , by $\lambda_{ee} = 3.86(E + V_0)^{1/2}/\beta$, where λ_{ee} is in Å and V_0 , E , and β in eV. (The electron mean free path for phase coherence, λ_e , is related to λ_{ee} by $\lambda_e = \frac{1}{2}\lambda_{ee}$.) Note that above 40 eV the β for $\lambda_{ee} \sim 6.3$ or 8.3 Å is always greater than the β we find, and that $\beta = 4$ eV is too large below 100 eV, but too small above. The effects of these various forms of $\beta(E)$ on calculated spectra are illustrated in Fig. 7 and compared with experiment. Clearly, $\beta = 4$ eV not only gives relative amplitudes at low E (~ 50 eV) that are much too small compared to amplitudes at high E (120 eV) but also washes out and distorts the spectral structure observed near 30 eV. The calculation with $\lambda_{ee} \sim 6.3$ Å does a better job with relative intensities, but in general suppresses some of the observed structure at higher energies, e.g., the shoulders at 72, 85, and 110 eV in the $\phi = 45^\circ$ spectra. At low energies (~ 40 eV) $\lambda_{ee} \sim 8.3$ Å does well but at higher energies the structural features near 80 and 100 eV in the $\phi = 0^\circ$ spectra, as well as above 150 eV (not shown), become smeared out. Our $\beta(E)$ absorption function gives values of β (or λ_{ee}) which are similar to the values of β (or λ_{ee}) for $\lambda_{ee} \sim 8.3$ Å near 40 eV (± 20 eV) but which are smaller at higher energies. This gradual reduction in β above ~ 60 eV allows our $E^{1/3}$ absorption function to resolve more of the spectral features

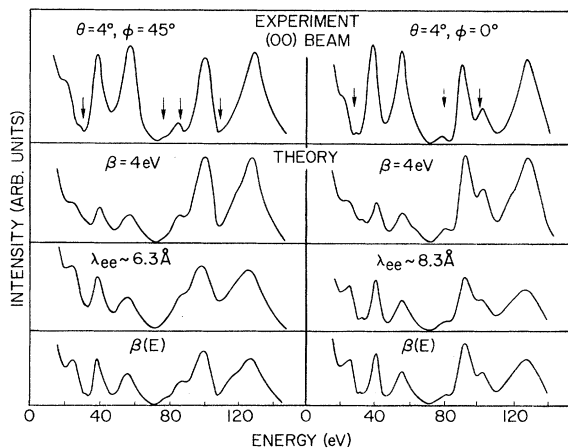


FIG. 7. Comparison of room-temperature experimental spectra on Ni(001) (Ref. 7) for the (00) beam at $\theta = 4^\circ$ and $\phi = 0^\circ$ and 45° with calculated spectra illustrating how the damping parameter affects the LEED spectra. Attention is focused on the fine structure marked by arrows in the experimental curves.

at higher energies (> 80 eV) than is possible for $\lambda_{ee} \sim 8.3$ Å. (We also point out that a constant λ_{ee} of nearly 10 Å corresponds closely to our $E^{1/3}$ absorption function between 100 and 200 eV.) It should be noted that at very low energies (near ~ 20 eV) the use of a monotonically varying absorption function becomes questionable due to a threshold for interband and possibly even plasmon excitations which will modify electron absorption. We expect that at these low energies our absorption function should not be applicable. Similarly at higher energies, if other discrete electron absorption processes start to occur at some energy threshold, we would expect to see departures in the calculated LEED spectra from experiment (due our choice of a monotonically varying absorption function). In fact, we later discuss a particular feature in our comparisons that indicate that such an absorption threshold occurs near 65 eV.

The accuracy of our method of calculation is not affected by the magnitude of the absorption. In perturbation methods, where only a limited number of scattering events is considered,^{4,10-12} and in methods which consider a finite number of layers^{5,8} the choice of absorption becomes an important consideration. In the former, the choice of absorption may be artificially high so as to permit convergence of the calculation. In the latter, the electron penetration length (i.e., the absorption) sets requirements on the number of layers to be considered so as to make the model of the surface realistic. These effects deserve attention.

III. COMPARISON OF THEORY TO EXPERIMENT

Having determined suitable input parameters, we now compare calculated intensity energy spectra to those measured experimentally. We show only calculations where experimental data are available, although we have calculated up to 47 diffraction beams for each sample orientation. The nomenclature regarding crystal azimuth and diffraction beams is identical to that reported in the experimental work of Demuth and Rhodin.⁷ Figure 8 illustrates three important features of the calculation on (001) Ni: (i) the effect of varying the first interlayer spacing d_1 of the (001) surface by 5, 2.5, 0, -2.5, and -5% from the expected interlayer (001) spacing for a bulk crystal ($a_0 = 3.517$ Å); (ii) the ability of the LEED calculation to reproduce the line shapes for a spectrum which shows highly nonkinematic characteristics; (iii) the structural features of even the highest-energy peak shown in Fig. 8 are strongly dependent on interlayer spacing.

From the details of the calculated line shapes in Fig. 8 for the highest-energy peak near 180 eV it appears that a very good match to the experi-

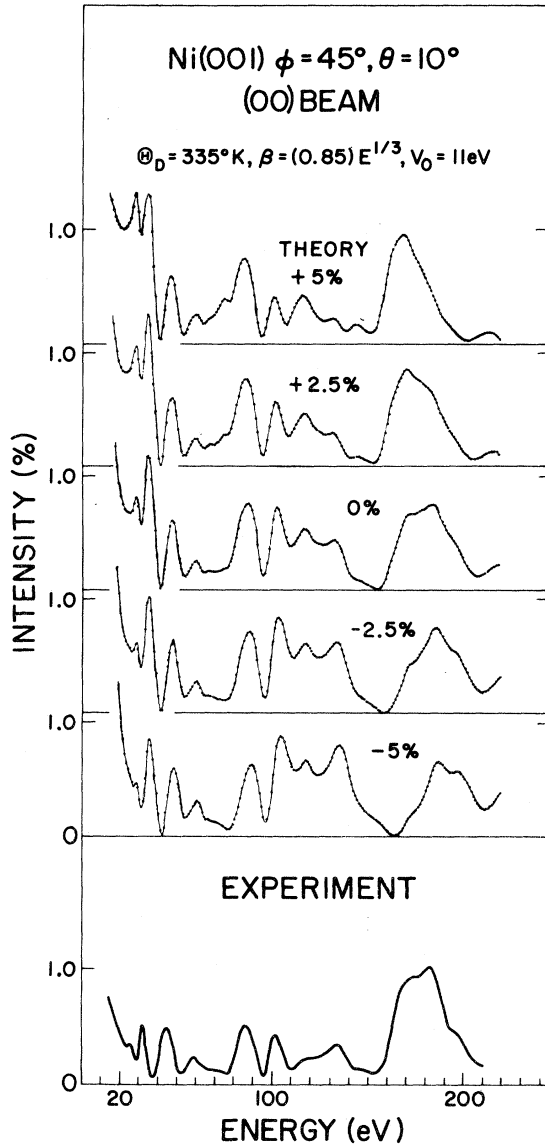


FIG. 8. Comparison of the experimental spectra of Demuth and Rhodin (Ref. 7) for the (00) beam on Ni(001) for $\theta = 10^\circ$ and $\phi = 45^\circ$ with calculated spectra in which the first interatomic (001) layer spacing d_1 has been expanded (+) or contracted (-) from the expected "bulk" (100) interlayer spacing of $\sim 1.76 \text{ \AA}$. Identical Debye temperatures of 335°K , an inner potential of 11 eV , and damping of the form $\beta = 0.85E^{1/3}$ were used in this and all following calculations.

mental spectrum occurs for the unexpanded surface. Further comparisons for the (00) beam for different angles along two azimuths and for the nonspecular (01) and (11) beams are shown in Figs. 9–12. In general our unexpanded calculation describes the experimental spectra for the (001) surface very well. However, the data for $\theta = 6^\circ$, $\phi = 45^\circ$ for the (00) beam, as well as for the (11)

beam, fit better for a lattice expansion of 2.5% or 0.04 \AA from the normal bulk interlayer spacing of $\sim 1.76 \text{ \AA}$. Thus we conclude that d_1 may be expanded from the ideal (001) surface between 0 and 2.5% or $\sim 0.02 \pm 0.02 \text{ \AA}$. Figures 11 and 12 also show that the experimental spectra obtained by Demuth and Rhodin⁷ and Andersson and Kasemo³⁴ on Ni(001) have nearly identical spectral features but have different measured intensities relative to one another.

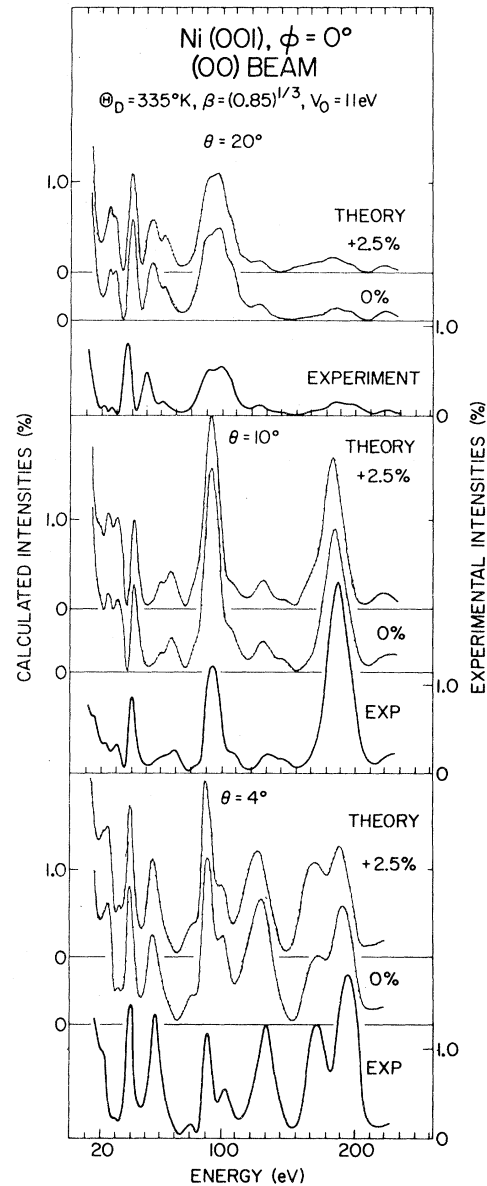


FIG. 9. Comparison of the experimental spectra of Demuth and Rhodin (Ref. 7) for the (00) beam on Ni(001) for $\theta = 4^\circ, 10^\circ,$ and 20° along the $\phi = 0^\circ$ azimuth with calculated spectra for a normal first interlayer spacing and one which has been expanded by 2.5% or $\sim 0.04 \text{ \AA}$.

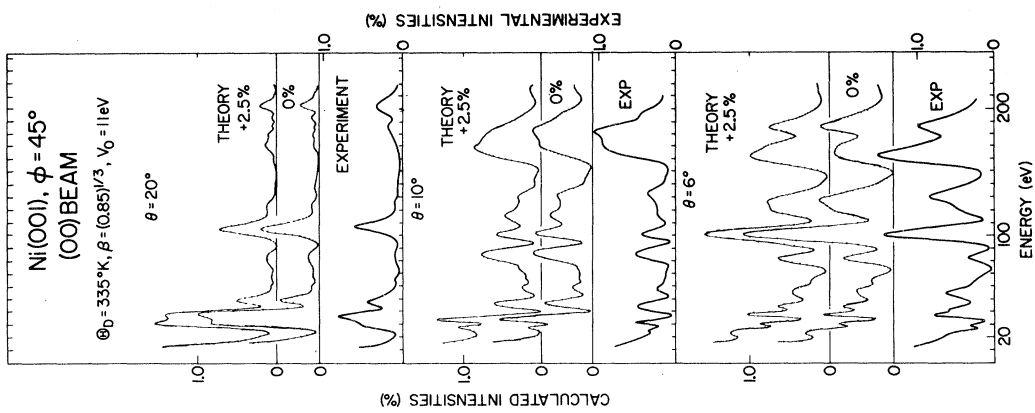


FIG. 10. Comparison of the experimental spectra of Demuth and Rhodin (Ref. 7) for the (00) beam on Ni(001) for $\theta = 4^\circ$, 10° , and 20° along the $\phi = 45^\circ$ azimuth with calculated spectra for a normal first interlayer spacing and one which has been expanded by 2.5% or $\sim 0.04 \text{ \AA}$.

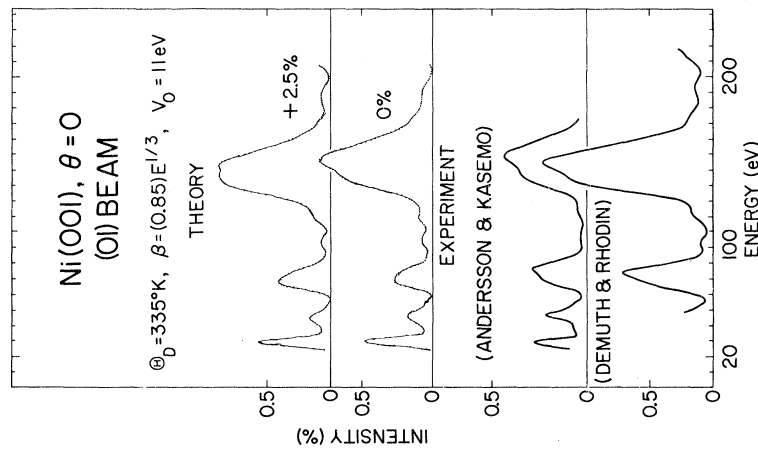


FIG. 11. Comparison of the room-temperature experimental spectra of Demuth and Rhodin (Ref. 7) and Andersson and Kasemo (Ref. 34) for the (01) beam at normal incidence with calculated spectra for a normal first interlayer spacing and one which has been expanded by 2.5% or $\sim 0.04 \text{ \AA}$.

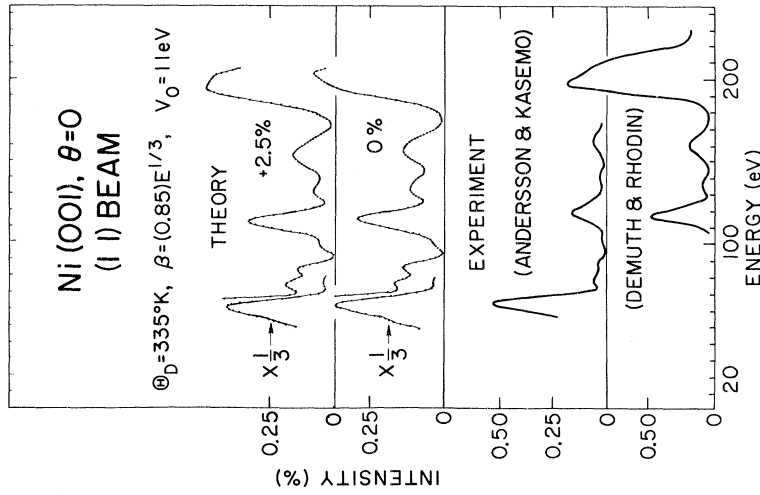


FIG. 12. Comparison of the room-temperature experimental spectra of Demuth and Rhodin (Ref. 7) and Andersson and Kasemo (Ref. 34) for the (11) beam at normal incidence with calculated spectra for a normal first interlayer spacing and one which has been expanded by 2.5% or $\sim 0.04 \text{ \AA}$.

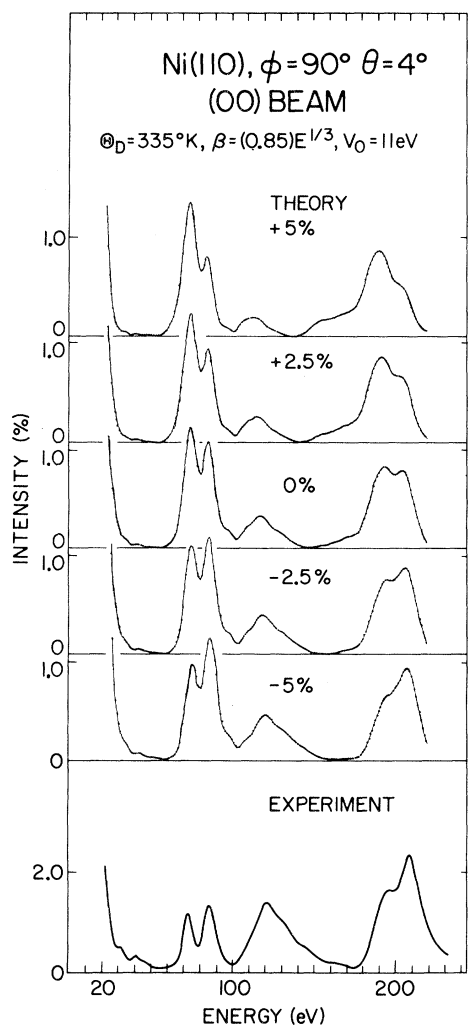


FIG. 13. Comparison of the experimental spectra of Demuth and Rhodin (Ref. 7) for the (00) beam on Ni(110) for $\theta=4^\circ$ and $\phi=90^\circ$ with calculated spectra where the first interatomic (110) layer spacing has been expanded (+) or contracted (-) from the expected "bulk" interlayer spacing of $\sim 1.24 \text{ \AA}$.

Using the same model parameters to calculate spectra for the (110) Ni surface we again observe, as shown in Fig. 13, a marked sensitivity of the calculated spectra to d_1 . However, we now observe best matches for d_1 decreased from its bulk value. Our best agreement between the calculated and experimental spectra occurs for a 5% contraction of d_1 from the bulk value, as shown in Figs. 14 and 15, for the (00) beam along two different azimuths and in Figs. 16-18 for the (01), (10), and (11) beams at normal incidence. This contraction corresponds to a $0.065 \pm 0.02 \text{ \AA}$ reduction of d_1 from the expected bulk interlayer (110) spacing of ~ 1.24

\AA . A similar contraction of the (110) surface of Al was inferred from previous LEED calculations on Al,³⁵ although faceting, which was observed, could also produce changes in the spectra similar to surface contraction.³⁶ However, in the case of Ni(110) no such faceting was observed for either of the two samples studied.⁷ Thus, unlike the case of Al(110), a contraction of d_1 seems unambiguously indicated.

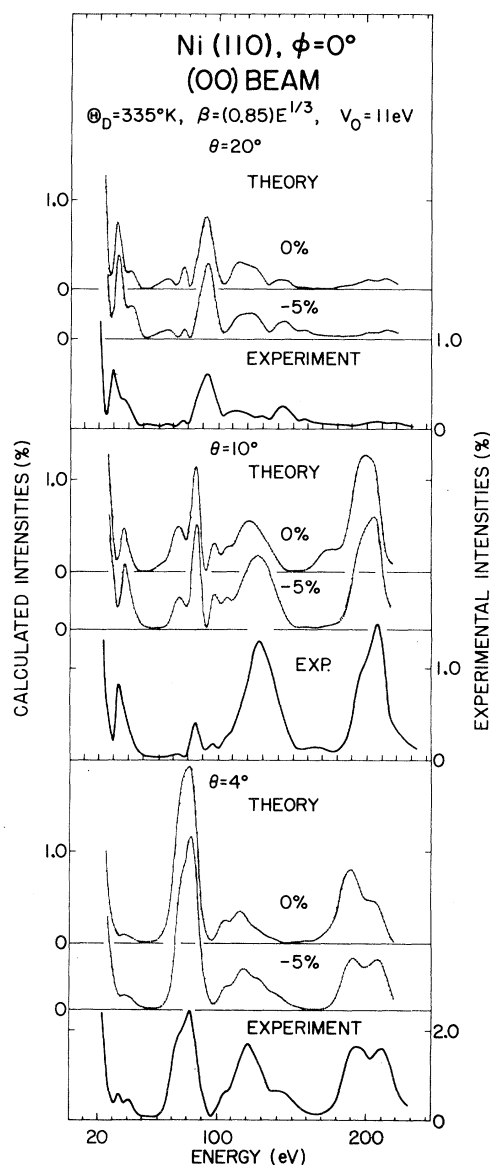


FIG. 14. Comparison of the experimental spectra of Demuth and Rhodin (Ref. 7) for the (00) beam on Ni(110) for $\phi=0^\circ$ and $\theta=4^\circ, 10^\circ,$ and 20° with calculated spectra for a normal first interatomic layer spacing and one which has been contracted 5% or $\sim 0.063 \text{ \AA}$.

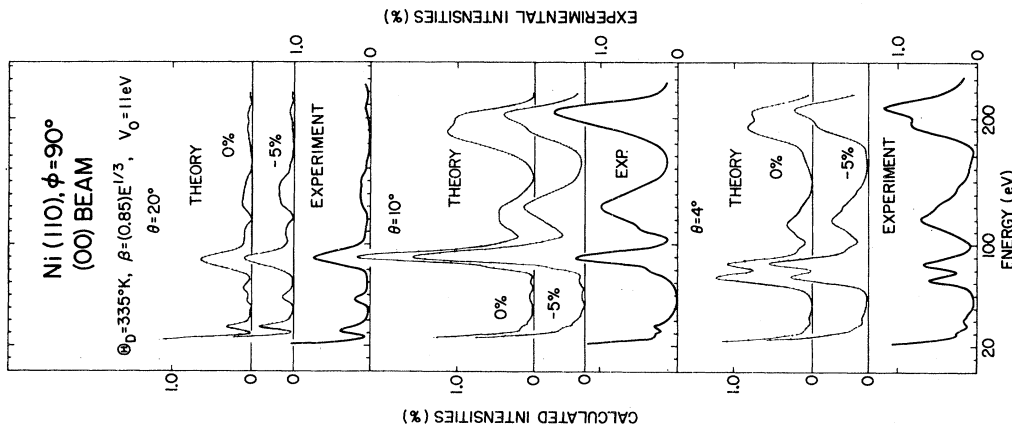


FIG. 15. Comparison of the experimental spectra of Demuth and Rhodin (Ref. 7) for the (00) beam on Ni(110) for $\phi = 90^\circ$ and $\theta = 4^\circ$, 10° , and 20° with calculated spectra for a normal first interatomic layer spacing and one which has been contracted 5% or $\sim 0.063 \text{ \AA}$.

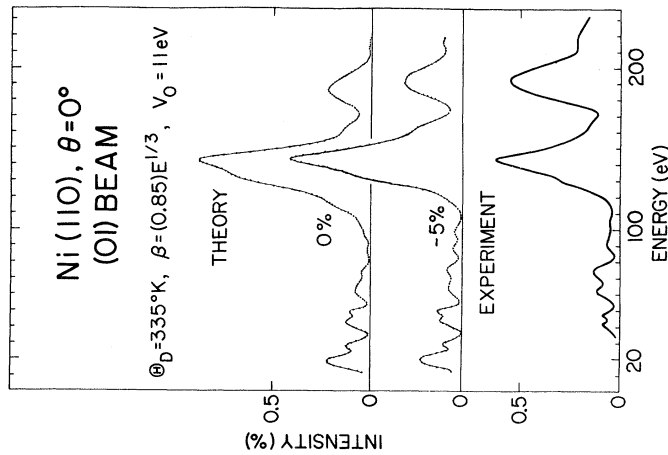


FIG. 16. Comparison of the experimental spectra of Demuth and Rhodin (Ref. 7) for the (01) beam on Ni(110) at normal incidence with calculated spectra for a normal first interatomic layer spacing and one which has been contracted by 5% or $\sim 0.063 \text{ \AA}$.

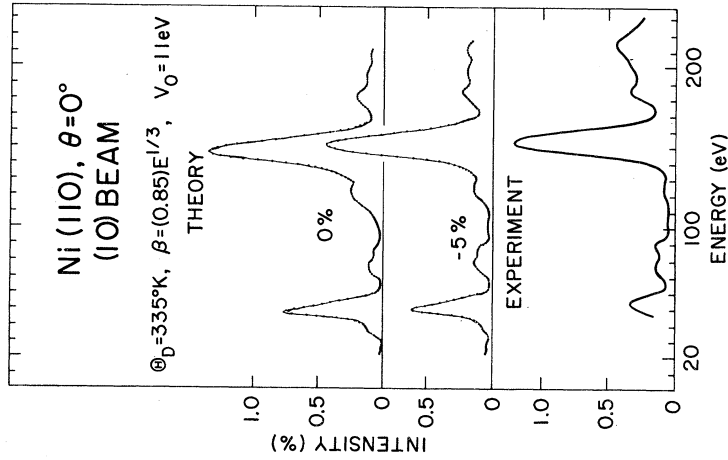


FIG. 17. Comparison of the experimental spectra of Demuth and Rhodin (Ref. 7) for the (10) beam on Ni(110) at normal incidence with calculated spectra for a normal first interatomic layer spacing and one which has been contracted by 5% or $\sim 0.063 \text{ \AA}$.

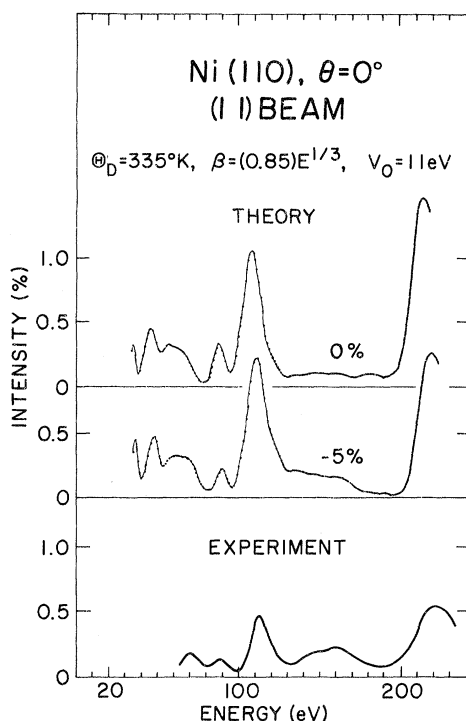


FIG. 18. Comparison of the experimental spectra of Demuth and Rhodin (Ref. 7) for the (11) beam on Ni(110) at normal incidence with calculated spectra for a normal first interatomic layer spacing and one which has been contracted by 5% or $\sim 0.063 \text{ \AA}$.

Application of the same procedure to the (111) surface again displays a strong sensitivity of the calculated spectra to the size of d_1 as shown in Fig. 19. The best agreement of spectral line shapes here occurs for the unrelaxed surface. The comparison of (00), (10), and $(\bar{1}0)$ beam spectra is shown in Figs. 20–22 for the ideal unrelaxed surface (0%) and for d_1 contracted by 2.5%. For the (10) and $(\bar{1}0)$ beams we compare our calculations to the experimental results of Park and Farnsworth³⁷ and Demuth and Rhodin,⁷ which are structurally identical in their regions of overlap. Based upon these comparisons, we conclude that d_1 for the (111) surface may be contracted by up to $0.025 \pm 0.025 \text{ \AA}$ from the bulk value of 2.03 \AA .

IV. DISCUSSION OF RESULTS

We have shown that the agreement between calculated and measured LEED spectra is quite good for all three faces of Ni using identical model parameters. However, there are still systematic discrepancies that provide further information about the scattering process and effective potential. As previously mentioned, our inner potential of 11 eV was based on an over-all best fit of peak

positions for the (001) surface, but there are systematic deviations Δ between calculated and experimentally observed peak positions. We now determine Δ as a function of E , using the value of the first interlayer spacing which allows the best match between calculated and experimental spectral structure. As demonstrated in Figs. 8, 13, and 19, knowledge of this interlayer spacing is important *a priori*, since changes in the interlayer

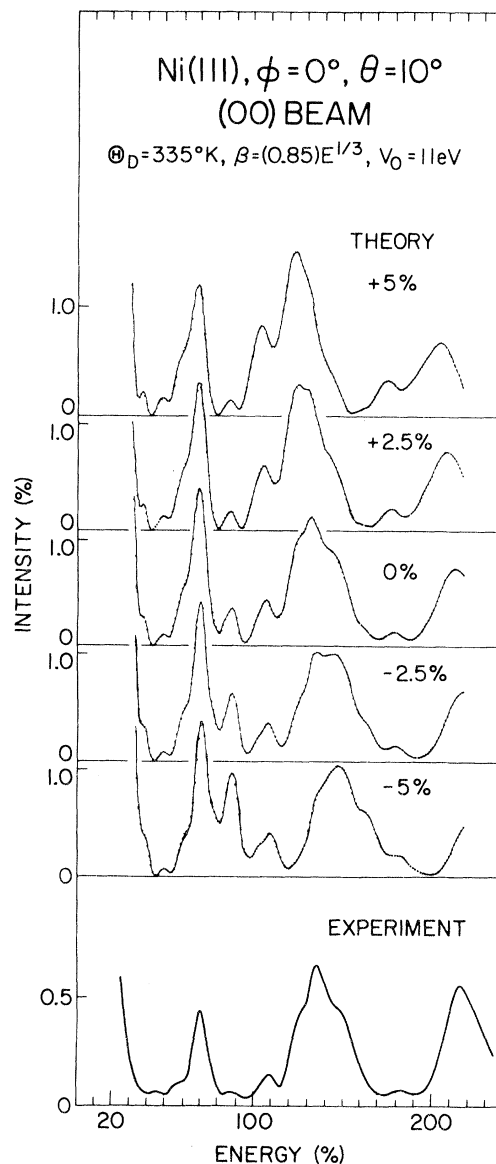


FIG. 19. Comparison of the experimental spectral of Demuth and Rhodin (Ref. 7) for the (00) beam on Ni(111) for $\theta=10^\circ$ and $\phi=0^\circ$ with calculated spectra where the first interatomic layer spacing has been expanded (+) or contracted (-) from the expected bulk (111) interlayer spacing of $\sim 2.03 \text{ \AA}$.

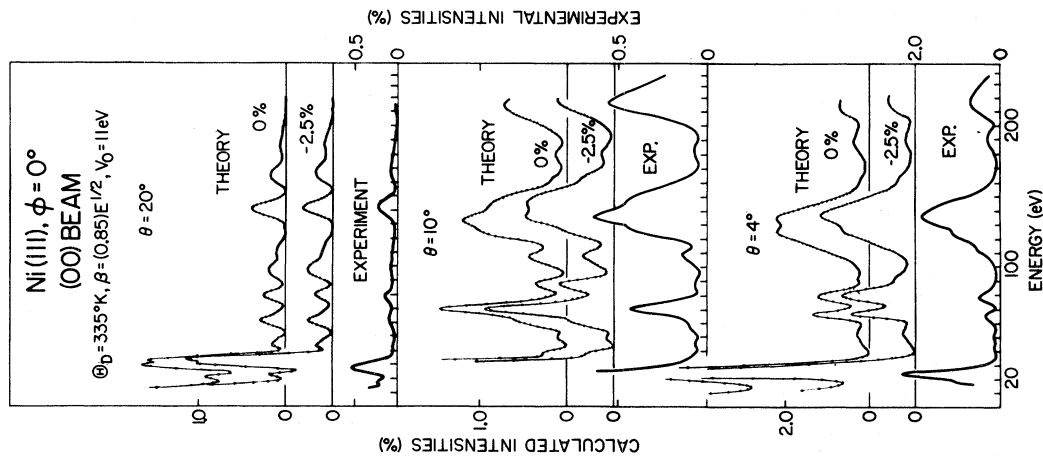


FIG. 20. Comparison of the experimental spectra of Demuth and Rhodin (Ref. 7) for the (00) beam on Ni(111) for $\phi = 0^\circ$ and $\theta = 4^\circ, 10^\circ$, and 20° with calculated spectra for a normal first interatomic layer spacing of 2.03 Å and one which has been contracted 2.5% or 0.05 Å.

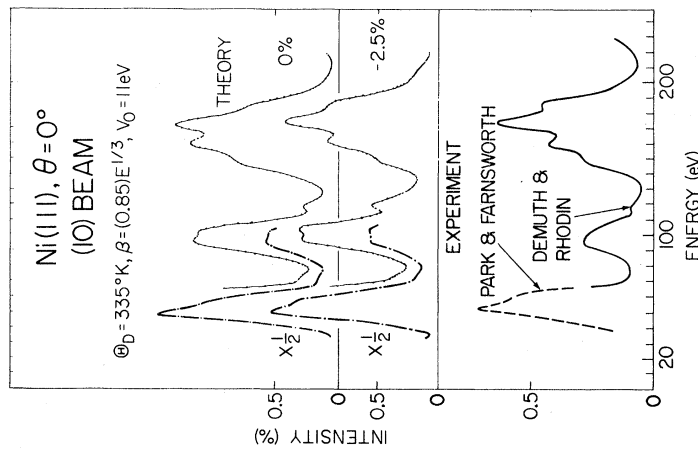


FIG. 21. Comparison of the experimental spectra of Demuth and Rhodin (Ref. 7) (solid line) and Park and Farnsworth (Ref. 37) (dashed line) for the (10) beam on Ni(111) at normal incidence with calculated spectra for a normal first interatomic layer spacing and one which has been contracted 2.5% or ~ 0.05 Å. The experimental intensity of the dashed line is based upon matching peak intensities to that of Demuth and Rhodin (Ref. 7).

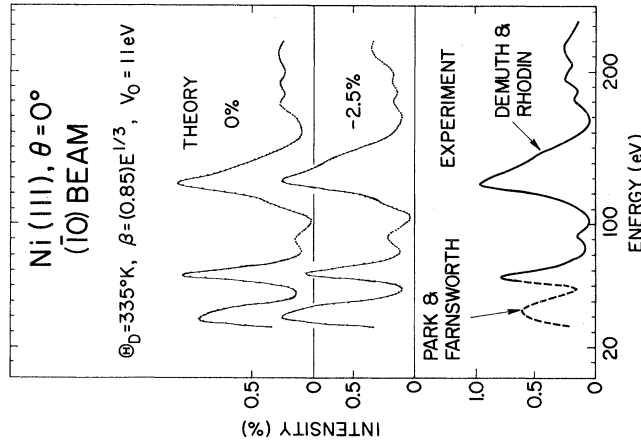


FIG. 22. Comparison of the experimental spectra of Demuth and Rhodin (Ref. 7) (solid line) and Park and Farnsworth (Ref. 37) (dashed line) for the (10) beam on Ni(111) at normal incidence with calculated spectra for a normal first interatomic layer spacing and one which has been contracted 2.5% or ~ 0.05 Å. The experimental intensity of the dashed line is based upon matching peak intensities to that of Demuth and Rhodin (Ref. 7).

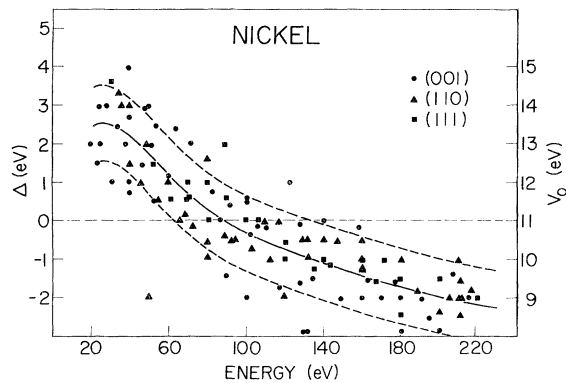


FIG. 23. Comparison of the displacements in peak positions, Δ (left scale), between experimental and calculated spectra for an assumed 11-eV inner potential for all surfaces. The energy-dependent inner potential (solid line) which would be needed to align calculated and experimental peak positions with a standard deviation of ~ 0.75 eV can be read from the scale on the right. (The dashed line corresponds to the solid line ± 1 eV.)

spacings also cause significant displacements in peak positions. Figure 23 shows $\Delta(E)$ and the corresponding values of inner potential $V_0(E)$ which would allow matching of experimental and calculated peak positions. At the lowest energies we observe an inner potential of ~ 13.5 eV, consistent with our expectations based upon our knowledge of the work function and the position of the muffin-tin zero of the Wakoh potential relative to the Fermi level. However, at higher energies V_0 appears to decrease and then to level off at ~ 9 eV for incident-electron energies of ~ 220 eV. The over-all standard deviation of the experimental peak positions from our $V_0(E)$ curve is about 0.75 eV. The energy dependence of V_0 , as we have anticipated, is consistent with a decrease in electron correlation for electrons of higher kinetic energy which does, in fact, reduce the effective surface barrier. Due to the spread of the points in Fig. 24 we cannot determine differences in the inner potential for different crystal surfaces.

Previous calculations by Laramore⁸ and Tong and Kesmodel⁶ using matrix inversion techniques for five layers and five phase shifts indicate that an inner potential of 14 eV appears to allow matching of calculated and experimental peak positions up to 220 eV. The calculations in Fig. 1 show that use of only five phase shifts produces an apparent displacement in the positions of the higher-energy peaks to higher energies. This displacement of peaks for the five-phase-shift calculation roughly cancels the reduction in V_0 at higher energies which we find, and, as noted by Tong,⁶ explains why a constant inner potential of 14 eV appears adequate for Ni in these previous calculations. Our initial choice of

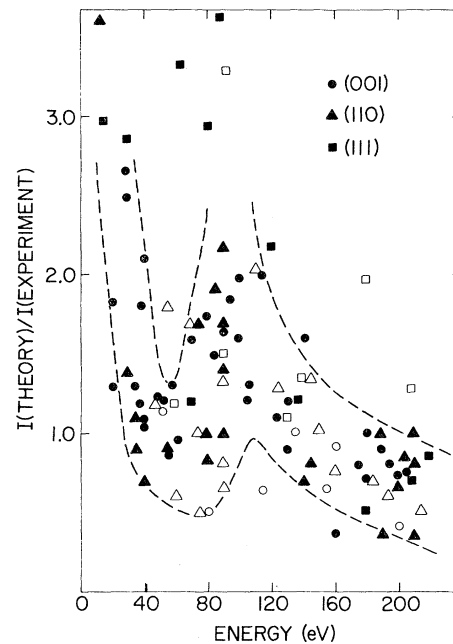


FIG. 24. Comparison of the ratio of theoretical and experimental diffraction peak intensities as a function of energy on all crystal faces. The solid data points are for specular beam diffraction peaks, while the open data points are for nonspecular beam peaks.

$V_0 = 11$ eV represents an average inner potential observed for Ni(001) between 20 and 150 eV, which from Fig. 23 also appears to be a reasonable average inner potential for the (110) and (111) surfaces.

Although features of the diffraction model as well as several experimental uncertainties in obtaining "absolute" intensities make it difficult to compare the actual and experimental absolute intensities, the energy dependence of the relative intensities between theory and experiment should provide additional physical insight into those processes which are affecting diffraction intensities. In Fig. 24 we compare the ratio of calculated to measured intensities for various diffraction peaks on all three surfaces; we find, interestingly, a nonmonotonic variation of the ratio for all surfaces. (We do not distinguish any differences in the trends of this ratio for specular versus nonspecular beams.) Since the model calculation contains parameters which vary only monotonically with energy, such as the inner potential or electron damping, this nonmonotonic variation with energy appears to require some phenomenon which markedly reduces the experimental intensities for electrons with kinetic energy above about 65–70 eV (measured relative to the vacuum level). We note that measured core levels³⁸ and soft-x-ray absorption thresholds³⁹ show the "core" excitation of $3p$ electrons from nickel to occur at ~ 68 eV. At such a core-level threshold the electron attenuation

by the crystal would increase and the elastic diffraction intensity decrease. We thus attribute the decrease in experimental intensities at ~ 65 eV to excitation of $3p$ electrons from nickel. Since this core-level excitation markedly affects diffraction intensities, it would appear necessary to include such inelastic-scattering thresholds in electron-damping models if further detailed analysis of the LEED intensities is to be made. From the dependence of the intensity upon β , we estimate roughly that this threshold increases our proposed β from 3.6 eV ($\lambda_{ee} \approx 9.2$ Å) at 60 eV to a maximum value of about ~ 5 –5.5 eV ($6.5 < \lambda_{ee} < 7.4$ Å) near 90 eV and then returns to the $E^{1/3}$ variation in β at 110 eV ($\beta = 4.1$ eV, $\lambda_{ee} = 10$ Å).

In addition to this $3p$ absorption threshold of Ni, we observe that the ratio of intensities decreases rapidly at low energies with increasing energy and slowly at high energies. At low energies (below ~ 30 eV) on the (001) surface our calculation may overemphasize the structural features observed in the experiment; i. e., the assumed λ_{ee} may be too large below about 30 eV. However, the model used does not allow for barrier scattering, which also affects the intensity ratio at these low energies. In addition, at the lower energies the bulk scattering potential used may not be adequate for the surface region, since nonspherical corrections to this muffin-tin potential may be necessary to account properly for the valence-electron charge distribution. (The valence charge of the atom is more important for electron scattering at low electron energies than at higher energies.)

At higher electron energies (> 120 eV) the absorption appears to have returned to our proposed $\beta = 0.85E^{1/3}$ absorption function. It is believed that the experimentally measured intensities above 150 eV include quasielastic contributions which would tend to increase measured intensities up to $\sim 20\%$,⁷ and therefore reduce the ratio of calculated to measured intensities, as observed in Fig. 24. In addition, as we have previously noted, a layer-averaged Debye temperature of 335 °K may underestimate intensities at these energies.

The over-all agreement of calculated peak intensities with the experimental results of Demuth and Rhodin⁷ to within a factor of 2 may be considered somewhat fortuitous. As we have commented earlier, differences between the experimental results of Andersson and Kasemo³⁴ and Demuth and Rhodin⁷ are at least a factor of 2 different for Ni(001), and even larger differences exist between this latter group's measurements on Ni(111) and those of Legally, Ngoc, and Webb.^{31,40} In view of these experimental uncertainties, as a result of differences in both sample preparation (surface roughness) or electron beam coherence zones which are not included in the calculation, there can be little signifi-

cance in comparing diffraction intensities on an absolute scale. It is for these reasons that we have stressed the use of line shapes and relative spectral feature intensities in comparing theory to experiment. However, our comparison of theory to internally consistent experimental results on all three faces of Ni can be used to obtain some physical insight into the relative intensity variations for different crystal faces. For example, at higher incidence angles on the (111) surface the calculated intensities near 100 eV are higher relative to experiment than at lower incident angles (see Fig. 20). Since this was not the case for the (001) or (110) surfaces, the (111) surface may have a particular type of surface defect which produces shadowing effects at higher incident angle, as postulated⁷ in previous experimental work. In general, the overall similarities in the ratio of calculated and experimental intensities at normal incidence for all surfaces might be expected, since all samples were experimentally prepared in a similar fashion and may have similar degrees of surface perfection.

V. SUMMARY AND CONCLUSIONS

We have demonstrated that the model used here to calculate low-energy-electron-diffraction spectra from Ni can very adequately describe the room-temperature experimental results of both Demuth and Rhodin⁷ and Andersson and Kasemo.³⁴ The four model parameters [Θ_D , $\beta(E)$, d_1 , and $V_0(E)$] have been determined from experimentally observed features of the intensity spectra. Our analysis, which stresses matching the *structural features* (rather than simply peak positions) in the experimental and calculated spectra, allows much basic physical information to be obtained from LEED spectra: (a) An effective average Θ_D of 335 °K is determined; (b) an absorption function $\beta(E) = 0.85E^{1/3}$ (in eV) is deduced; (c) the first interlayer spacing d_1 of the (001) surface is found to be expanded from its expected bulk value by 0.02 ± 0.02 Å, while the (110) and (111) surfaces are contracted by 0.06 ± 0.02 and 0.025 ± 0.025 Å, respectively; (d) the inner potential $V_0(E)$ needed to match calculated and experimental peak positions is determined to vary monotonically from 13.5 eV at low energies and level off at 9 eV at higher energies; and (e) based upon the *relative* variation of calculated to experimental intensities for all surfaces, a region of increased electron absorption with a threshold at about 65 eV is observed.

From the model parameters found here, it is now possible to examine with confidence overlayer structures on Ni via similar model calculations. Thus, the extension of such model calculations is in progress and has yielded detailed structural information regarding adsorbed atoms on nickel surfaces.⁴¹

- ¹J. B. Pendry, *J. Phys. C* **4**, 3095 (1971).
²D. W. Jepsen, P. M. Marcus, and F. Jona, *Phys. Rev. B* **5**, 3933 (1972).
³S. Y. Tong, T. N. Rhodin, and R. H. Tait, *Phys. Rev. B* **8**, 421 (1973).
⁴G. E. Laramore and C. B. Duke, *Phys. Rev. B* **5**, 267 (1972).
⁵S. Y. Tong and L. L. Kesmodel, *Phys. Rev. B* **8**, 3753 (1973).
⁶S. Y. Tong, *Solid State Commun.* (to be published).
⁷J. E. Demuth and T. N. Rhodin, *Surf. Sci.* **42**, 261 (1974).
⁸G. E. Laramore, *Phys. Rev. B* **8**, 515 (1973).
⁹S. Andersson and J. B. Pendry, *J. Phys. C* **6**, 601 (1973).
¹⁰R. H. Tait, S. Y. Tong, and T. N. Rhodin, *Phys. Rev. Lett.* **28**, 553 (1972).
¹¹T. N. Rhodin and P. K. Lee (unpublished).
¹²S. Y. Tong, G. E. Laramore, and T. N. Rhodin, *Phys. Rev. B* **8**, 5361 (1973).
¹³D. W. Jepsen, P. M. Marcus, and F. Jona, *Phys. Rev. Lett.* **26**, 1365 (1971).
¹⁴D. W. Jepsen, P. M. Marcus, and F. Jona, *Phys. Rev. B* **8**, 5523 (1973).
¹⁵E. G. McRae, *Surf. Sci.* **8**, 14 (1967); *J. Chem. Phys.* **45**, 3258 (1966).
¹⁶J. L. Beeby, *J. Phys. C* **1**, 82 (1968).
¹⁷P. M. Marcus and D. W. Jepsen, in *Proceedings of the Sixth Low-Energy-Electron-Diffraction Seminar*, Washington, D.C., April, 1972 (unpublished).
¹⁸G. E. Laramore, *Phys. Rev. B* (to be published).
¹⁹J. W. D. Connolly, *Phys. Rev.* **159**, 415 (1967).
²⁰S. Wakoh, *J. Phys. Soc. Jpn.* **20**, 1984 (1965).
²¹B. I. Lundquist, *Phys. Status Solidi* **32**, 273 (1969).
²²C. B. Duke and G. E. Laramore, *Phys. Rev. B* **2**, 4765 (1970).
²³G. E. Laramore and C. B. Duke, *Phys. Rev. B* **2**, 4783 (1970).
²⁴D. W. Jepsen, P. M. Marcus, and F. Jona, *Surf. Sci.* **41**, 223 (1974).
²⁵A. U. MacRae and L. H. Germer, *Phys. Rev. Lett.* **8**, 489 (1962).
²⁶A. U. MacRae, *Surf. Sci.* **1**, 319 (1964).
²⁷S. Andersson and B. Kasemo, *Solid State Commun.* **8**, 1885 (1970).
²⁸R. H. Wilson, E. F. Skelton and J. L. Katz, *Acta Cryst.* **21**, 635 (1966).
²⁹F. N. Herbstein, *Advan. Phys.* **10**, 313 (1961).
³⁰B. C. Clark, R. Herman, and R. F. Wallis, *Phys. Rev.* **139**, A860 (1965).
³¹C. J. Powell, *Surf. Sci.* **44**, 29 (1974).
³²M. G. Lagally and M. B. Webb, in *The Structure and Chemistry of Surfaces*, edited by G. A. Somorjai (Wiley, New York, 1969).
³³The measured integrated intensities would probably not be low for the same reasons which cause the individually measured beam intensities to be low since these two measurements are made differently (see Ref. 31).
³⁴S. Andersson and B. Kasemo, *Surf. Sci.* **25**, 273 (1971).
³⁵D. W. Jepsen, P. M. Marcus, and F. Jona, *Phys. Rev. B* **6**, 3684 (1972).
³⁶G. E. Laramore, J. E. Houston, and R. L. Park, *J. Vac. Sci. Technol.* **10**, 196 (1973).
³⁷R. L. Park and H. E. Farnsworth, *Surf. Sci.* **2**, 527 (1964).
³⁸K. Siegbahn *et al.*, *Electron Spectroscopy for Chemical Analysis* (Almqvist and Wiksells Boktryckeri AB, Uppsala, 1967).
³⁹B. Sonntag, R. Haensel, and C. Kunz, *Solid State Commun.* **7**, 597 (1969).
⁴⁰M. G. Lagally, T. C. Ngoc, and M. B. Webb, *J. Vac. Sci. Technol.* **9**, 645 (1972).
⁴¹See, for example, J. E. Demuth, D. W. Jepsen, and P. M. Marcus, *Phys. Rev. Lett.* **31**, 540 (1973); **32**, 1187 (1974); *J. Phys. C* **8**, L25 (1975).